μFLU10-212

INFLUENCE OF THE SURFACE FORCES ON THE APPARENT CONTACT ANGLE AT PARTIAL WETTING AND IN THE PRESENCE OF HEAT AND MASS TRANSFER

Vladislav Janeček[1], **Vadim S. Nikolayev**
janecek.vladislav@espci.fr, vadim.nikolayev@espci.fr
ESEME, PMMH - ESPCI and SBT/INAC/CEA, 10 rue Vauquelin, 75005 Paris, France

KEY WORDS

evaporation, partial wetting, contact angle, disjoining pressure

ABSTRACT

The partial wetting conditions are met in different situations such as bubble growth in boiling, meniscus evaporation in capillaries or drop evaporation on a heated substrate. Unlike the complete wetting case, the wetting film is absent here and the actual line of the triple gas-liquid-solid contact appears. The present theoretical work deals with the evaporation of a fluid wedge in contact with its saturated vapor. A constant temperature higher than the saturation temperature is imposed at the substrate side opposite to the liquid. The gas-liquid interface is curved and its slope varies at the nanometric scale. Farther from the contact line, the slope becomes constant and defines the apparent contact angle. It is assumed to be small enough so that the lubrication approximation can be applied to describe the fluid dynamics. The apparent contact angle is different from both the Young contact angle and the microscopic contact angle (a small angle imposed at nanometer scale) because of two effects. The first is that of the surface forces accounted for by the disjoining pressure. The second effect is the hydrodynamic stress caused by the fluid flow. The contact line singularity is relaxed by introducing the Marangoni stress term and the slip length. A characteristic distance from the contact line, at which the apparent contact angle establishes (~ 1 μm), and the apparent contact angle itself are studied as functions of various microscopic parameters, imposed contact line velocity, and substrate temperature.

1. INTRODUCTION

Understanding of the mechanism of the liquid evaporation on a heated solid substrate is essential for modeling of the heat and mass transfer in non-isothermal microfluidic devices. Wedge-like geometry (Fig. 1) is quite common and appears at small scales near the liquid-gas-solid contact line in all main evaporation cases such as: bubble attached to a solid substrate (nucleate boiling), liquid meniscus in a capillary or sessile drop deposited on a substrate. In all these geometries there is a liquid wedge-shaped layer confined between the heated substrate and the gas-liquid interface. It is well known that this is a region where a dominant part of the evaporation occurs. For this reason we consider here the wedge geometry and assume that the liquid meniscus matches its macroscopic shape at a larger scale. When the gas is the saturated vapor corresponding to the liquid, the evaporation dynamics is controlled by the supplied heat flux spent mainly to compensate the latent heat of vaporization. In the wedge-like geometry, a stationary regime can be attained: the liquid can be supplied to the meniscus to compensate exactly the evaporation losses. The stationary regime is studied actively both theoretically and experimentally, see e.g. [1–3], because it allows the apparent contact angle to be defined as a function of external parameters. The effect of the contact line velocity can be studied in this geometry by assuming that the liquid wedge is steady but the substrate is moving.

[1] Corresponding author

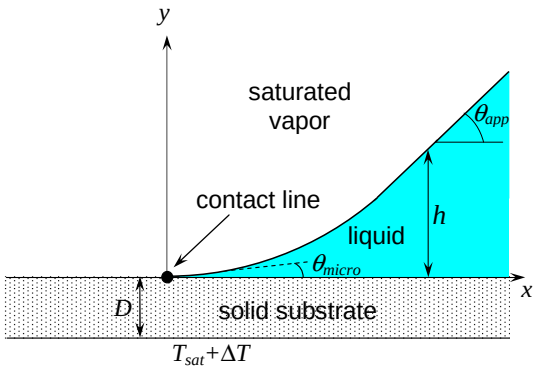

Figure 1: Wedge-like geometry.

The present understanding of the film evaporation phenomena is based on the approach developed originally by Wayner et al. [1] for the evaporation of the continuous liquid meniscus. In these theoretical and numerical studies it was assumed that the solid surface is covered by the continuous liquid film (called adsorption film or microlayer) that does not evaporate because of the van der Waals forces. This situation corresponds to the complete or pseudo-partial [4] wetting regimes.

It is well known that as the temperature grows, the van der Waals forces become weaker, and the adsorbed film may disappear. In this case a direct contact of vapor with the dry solid occurs and a triple vapor-liquid-solid contact line (CL) appears. This corresponds to the partial wetting regime (finite contact angle). Such a configuration may occur in situations of high practical importance. It was observed for example that for water a transition to the partial wetting situation occurs when the temperatures of the substrate is above $\sim 60°$C [5]. As in the continuous microlayer case, high heat fluxes occur in the vicinity of the CL. Following [6], we call this vicinity "microregion".

2. SURFACE FORCES IN THE PARTIAL WETTING CASE

The complete wetting case is simple to be understood basing on the long-range molecular attraction [7]. For this reason it is well studied. The occurrence of the partial wetting case is less evident. Its fundamentals are described in [4, 8]. We summarize it briefly in this section. Let us first consider the energy of a thin liquid film on the top of a solid substrate surrounded by a gas at equilibrium. The energy W per unit area is

$$W(h) = \sigma_{SL} + \sigma + P(h). \tag{1}$$

The first two terms are the tensions of the solid-liquid and gas-liquid interfaces, respectively. The term $P(h)$ is a contribution of the differential interaction energy of the molecules of the liquid and of the gas with those of the solid, which are called sometimes the thin film forces [7]. This term appears because the molecules of the solid "feel" the interface when $h \to 0$. The scale at which this phenomenon has a indispensable influence depends mainly on combination of materials in given system. Obviously, $P(h \to \infty) = 0$.

The case $h \to 0$ may be attained at partial wetting at the CL and for this reason needs to be discussed. It is evident that $W(h \to 0)$ has to be finite in this case. It has been postulated in [4] that

$$W(h \to 0) = \sigma_{SG}, \tag{2}$$

which corresponds to the energy of the dry (bare) solid-gas interface. Equations (1, 2) lead to $P(h \to 0) = S$, where

$$S = \sigma_{SG} - \sigma_{SL} - \sigma \tag{3}$$

is the spreading coefficient. A more general case $P(h \to 0) \neq S$ has been considered in [9]. This inequality can be justified by the existence of a monolayer that may modify the surface energy so that $W(h \to 0) \neq \sigma_{SG}$.

Consider the wedge-like geometry (Fig. 1). It can be shown that Young's contact angle θ_Y is $\cos\theta_Y = 1 + S/\sigma$ and the microscopic contact angle θ_{micro} formed at the scale of several nm is defined by

$$\cos\theta_{micro} = 1 + \frac{S - P(h \to 0)}{\sigma} \equiv \cos\theta_Y - \frac{P(h \to 0)}{\sigma}. \tag{4}$$

Note that the case (2) results in $\theta_{micro} = 0$. Once θ_Y, θ_{micro} and $P(h)$ are defined, the equilibrium gas-liquid interface shape can be obtained from the equation, see [4, 8]

$$\Delta p = K\sigma + \Pi(h), \tag{5}$$

where Δp is the pressure jump across the interface, $K \approx \partial^2 h/\partial x^2$ is the interface curvature in the small slope approximation and Π is the disjoining pressure related to P via

$$\Pi = -\frac{\mathrm{d}P}{\mathrm{d}h}. \tag{6}$$

At equilibrium, Δp does not vary along the interface. Since $\Pi(h \to \infty) = 0$ and $K(x \to \infty) = 0$,

$$\Delta p = 0. \tag{7}$$

It is necessary to note that the above approach has been developed in the "local" approximation, where P is assumed to be independent of the spatial variation of h. More sophisticated approach (where P is considered to be a functional of $h(x)$) is developed in [10] and gives a correction to (4, 5) at large θ_Y. In particular, $\theta_{micro} \neq 0$ even for $P(h \to 0) = S$. For small angles, the results of [10] are essentially similar to those of the local approach.

3. DISJOINING PRESSURE CHOICE

To perform the calculations, the function $\Pi(h)$ is required. The experimental data for h smaller than several nm are extremely rare and are unknown to us for the metal substrates of interest. Therefore we need to choose a form compatible with the system under study and with the partial wetting condition (4) that puts a constraint on the value $P(h \to 0)$. For large h (say, for $h > d_D$ where d_D is of nanometer scale), we adopt a conventional form of $\Pi(h)$ that appears due to the dispersion intermolecular forces [7],

$$\Pi = \frac{A}{6\pi h^3}. \tag{8}$$

The Hamaker constant A is positive for the case of "high - energy" metal surfaces.

We have chosen the simplest form compatible at the same time with (4), and (8),

$$\Pi(h) = \begin{cases} ah + b & \text{if } h \in (0, d_D) \\ \frac{A}{6\pi h^3} & \text{if } h \in (d_D, \infty) \end{cases}. \tag{9}$$

where d_D defines the position of the $\Pi(h)$ maximum. Once θ_Y, θ_{micro} are fixed, the coefficients a, b need to be chosen in such a way that $\Pi(h)$ is continuous and

$$P(h \to 0) \equiv \int_0^\infty \Pi(h)\mathrm{d}h \tag{10}$$

satisfies (4). The resulting disjoining pressure shape is shown in Fig. 2 together with the corresponding energy $P(h)$.

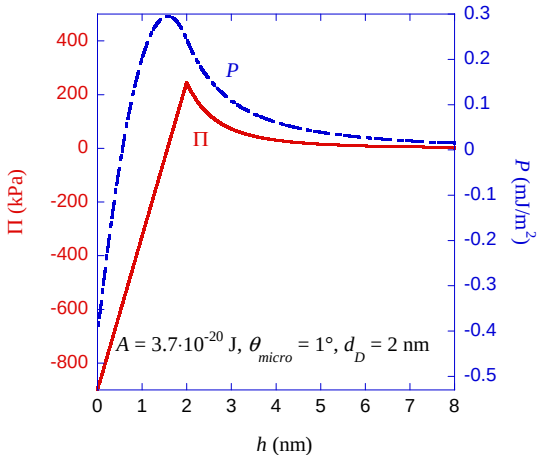

Figure 2: Example of the disjoining pressure shape.

4. HEAT TRANSFER IN THE MICROREGION

At equilibrium, the liquid-vapor interface temperature T^i_{eq} is well known to obey the Clausius-Clapeyron equation, which accounts for the interface pressure jump $\Delta p = p_V - p_L$,

$$T^i_{eq} = T_{sat}\left(1 + \frac{\Delta p}{H\rho_L}\right), \tag{11}$$

where p_V and p_L are the pressures at the vapor and liquid sides of the interface respectively; T_{sat} is the saturation temperature for the given p_V; H is the latent heat and ρ_L (ρ_V) is the liquid (vapor) density. In this work we adopt the "one-sided" description [1, 2, 6, 11, 12] according to which p_V is assumed to be spatially homogeneous. This hypothesis is justified by the smallness of both density and viscosity of the vapor. The interface temperature is allowed to vary along the interface together with p_L. When heat and mass exchanges at the interface are present, (11) remains to be valid because it is based on the hypothesis of the local equilibrium. It should however be augmented to account for the molecular kinetic effects by introducing the interface resistance [6]

$$R^i = \frac{T_{sat}\sqrt{2\pi R_g T_{sat}/M}(\rho_L - \rho_V)}{2H^2\rho_L\rho_V},$$

where M is the molar mass and R_g is the universal gas constant. The full expression for the interface temperature T^i reads

$$T^i = T_{sat}\left(1 + \frac{\Delta p}{H\rho_L}\right) + R^i q^i_L, \tag{12}$$

where q^i_L is the heat flux at the gas-liquid interface. The heater was supposed to be isothermal in many works on the meniscus evaporation [1,3,6,11]. However, q^i_L (and thus the evaporation rate) are then erroneous because in reality the heater temperature in the vicinity of the CL varies strongly as we shall see later on. In a more realistic modeling, the heat conduction in the heater needs to be taken into account. In this numerical study a *stationary* solution of the coupled hydrodynamic and heat transfer problems is considered. The validity of the stationarity assumption for the heat conduction problem will be evaluated later on. The following assumptions, usual for the "one-sided" description mentioned above, are adopted to solve the conjugated problem in the liquid and solid domains.

- The temperature distribution inside the liquid film is assumed to be stationary; a linear in y temperature variation is assumed. The heat flux is then independent of y so that the following equation is valid for $x \geq 0$:

$$q_S(x) = q^i_L(x) = k_L\frac{T_S(x) - T^i(x)}{h(x)}. \tag{13}$$

  Here $T_S(x)$ and $q_S(x)$ are the temperature and the heat flux at the substrate surface; k_L is the liquid heat conductivity.

- The vapor is assumed to be insulating so that the heat flux to the vapor domain is neglected,

$$q_S(x<0)=0. \tag{14}$$

This assumption leads also to the expression

$$HJ=q_L^i \tag{15}$$

valid at the vapor-liquid interface. Here J is the mass evaporation flux at the interface.
By combining (12, 13, 15), one obtains the expression

$$T_S(x)=T_{sat}\left[1+\frac{\Delta p(x)}{H\rho_L}\right]+q_S(x)\left[R^i+\frac{h(x)}{k_L}\right] \tag{16}$$

which describes the heat transfer in the liquid phase.

The 2D heat conduction problem

$$\nabla^2 T=0, \tag{17}$$

inside the infinite (along the x axis) solid heater of the thickness D is defined for the temperature $T=T(x,y)$. The temperature $T_{sat}+\Delta T$ is imposed at the bottom side of the heater $y=-D$ (Fig. 1), ΔT is called superheating. The first boundary condition at the top of the heater $y=0$ is given by the continuity of the temperature $T(x,0)=T_S(x)$, where T_S is defined by (16). The second boundary condition is the heat flux continuity $q_S(x)=-k_S\partial T(x,0)/\partial y$. The following expression valid for any x far from the contact line and any $y\in(-D,0)$ is easy to obtain,

$$T(x,y)=T_{sat}+\Delta T-\frac{q_S(x)}{k_S}(y+D). \tag{18}$$

Before solving numerically the solid domain problem, it is necessary to verify if its solution exists. The question is of importance because it is clear that the stationary heat conduction problem does not have a solution for example for $D\to\infty$. The question can be answered by checking the integrability of the Green function $G(x,y)$ that describes a temperature distribution created by a localized heat sink. One may place such a sink at the location of the CL $(0,0)$. The 2D Green function for the infinite space is then $G(x,0)=\log(x)$ and is not integrable when $x\to\infty$. This means that the stationary solution is nonexistent for $D\to\infty$ and the integrability of the Green function for the finite D needs to be verified. The Green function for the stripe $y\in(-D,D)$, $x\in(-\infty,\infty)$ and for the Dirichlet boundary conditions $G(y=\pm D)=0$ can be found in [13]. It is evident that such a problem is equivalent to that with the conditions $G(y=-D)=0$, $\partial G(y=0)/\partial y=0$ provided that the heat sink is situated at the symmetry plane $y=0$, which is the geometry and the boundary conditions appropriate for our case. The corresponding Green function is

$$G(x,0)=\frac{1}{2\pi}\log\left|\frac{\exp(\pi x/2D)-1}{\exp(\pi x/2D)+1}\right|\simeq-\frac{1}{\pi}\exp\left(-\frac{\pi x}{2D}\right). \tag{19}$$

It is obviously integrable at $x\to\infty$, which proves the existence of the stationary heat conduction solution.

An important conclusion can be deduced from (19). The decay of the temperature perturbation induced by the CL should be described far from it by the same function because of the strong localization of the contact line effects. This means that the perturbation is almost nonexistent for $|x|\gg D$, and the solution (18) can be used there.

There is another important consequence of the above analysis. Let us consider a characteristic length L of the temperature perturbation provided by the point heat sink. For the stationary heat conduction problem, $L\sim D$ according to (19). If one considers now a transient heat conduction problem, this length would be $L=\sqrt{\alpha\tau}$, where α is the thermal diffusivity of the solid. The typical time scale τ can be taken e.g. for the bubble growth at boiling $\tau\sim 1$ ms, which results in $L\sim 10$ μm. The heater temperature is thus perturbed at such a distance from the bubble. It means that for heater thicknesses $D\gg 10$ μm used in practice, the temperature perturbation does not have time to reach the stationary profile. This shows that D and $\sqrt{\alpha\tau}$ need to be compared in order to find out if the stationary heat conduction assumption is appropriate for the given physical system.

5. HYDRODYNAMICS IN THE MICROREGION

In the description of the micro-region, we restrict our consideration to the 2D case and than neglect the curvature of the vapor-liquid interface in the direction parallel to the CL with respect to the curvature K in the perpendicular direction. The interface can thus be described by its 2D contour (Fig. 1). It is assumed that the slope of the interface is small enough, $|\mathrm{d}h/\mathrm{d}x| \ll 1$. The lubrication approximation [14] can then be applied.

The boundary condition for the tangential fluid velocity v_x at the solid surface $y = 0$ is necessary to be defined among others. The simplest (and for this reason used by many researchers) method of relaxing this singularity consists in using instead of no-slip boundary condition the Navier slip condition

$$v_x = l_s \partial v_x / \partial y \tag{20}$$

that involves the slip length l_s. A conventional approach [14] shows that

$$\frac{\mathrm{d}}{\mathrm{d}x}\left[h\left(\frac{h}{2}+l_s\right)\frac{\mathrm{d}\sigma}{\mathrm{d}x}+h^2\left(\frac{h}{3}+l_s\right)\frac{\mathrm{d}\Delta p}{\mathrm{d}x}\right]=\mu\left(v^i-\frac{J}{\rho_L}\right), \tag{21}$$

where μ is the dynamic viscosity and the identity $\mathrm{d}\Delta p/\mathrm{d}x = -\mathrm{d}p_L/\mathrm{d}x$ is used. The interface velocity v^i is

$$v^i = v_{CL}\mathrm{d}h/\mathrm{d}x, \tag{22}$$

where v_{CL} is the CL velocity in x-direction. $v_{CL} > 0$ corresponds to the displacement of the substrate to the left in Fig. 1 (i.e. to the substrate dewetting). CL remains immobile in this reference. The linear dependence of the surface tension on the temperature is taken into account. Thus the Marangoni stress

$$\mathrm{d}\sigma/\mathrm{d}x = -\gamma \mathrm{d}T^i/\mathrm{d}x, \tag{23}$$

where T^i is defined in (12) and $\gamma = -\mathrm{d}\sigma/\mathrm{d}T$ is assumed to be constant. Note that γ is generally positive for pure fluids.

The h variation obeys (5). The boundary conditions at the CL $x = 0$ are given by two expressions,

$$h = 0, \tag{24}$$

$$\mathrm{d}h/\mathrm{d}x = \theta_{micro}. \tag{25}$$

Note that one needs solving two equations of second order (5, 21) with respect to x so that 4 boundary conditions are required. Two of them are (24, 25). In principle one more condition (7) imposed at $x \to \infty$ suffices. The fourth condition

$$\mathrm{d}\Delta p/\mathrm{d}x = 0 \tag{26}$$

is valid at $x \to \infty$ and is trivial because follows from (7). It is however useful in the numerical calculation where the infinite value of x should be replaced by a finite value x_{max}. In order to avoid a loss of accuracy because of full determination of the matrix resulting from (21) (i.e. smallness of its diagonal elements at small h), the following change of variables [15]

$$x = \exp(\zeta), \tag{27}$$

$$h = \chi \exp(\zeta), \tag{28}$$

is applied. The point $x = 0$ corresponds to $\zeta \to -\infty$. In numerical calculation the finite value of $\zeta_{min} \approx -15$ is chosen as is considered to be sufficiently small so that $h(\zeta_{min})$ is smaller than the smallest length scale of the problem.

6. NUMERICAL SOLUTION AND RESULTS

The solid domain problem (17) is solved with the Boundary Element Method (BEM) [13]. The Finite Volume method [16] is used to discretize the liquid domain equations (5, 21). A homogeneous mesh of 250 elements is used for the liquid domain $\zeta \in (\zeta_{min}, \ln x_{max})$. Such a mesh is increasingly dense when $x \to 0$, see Fig.

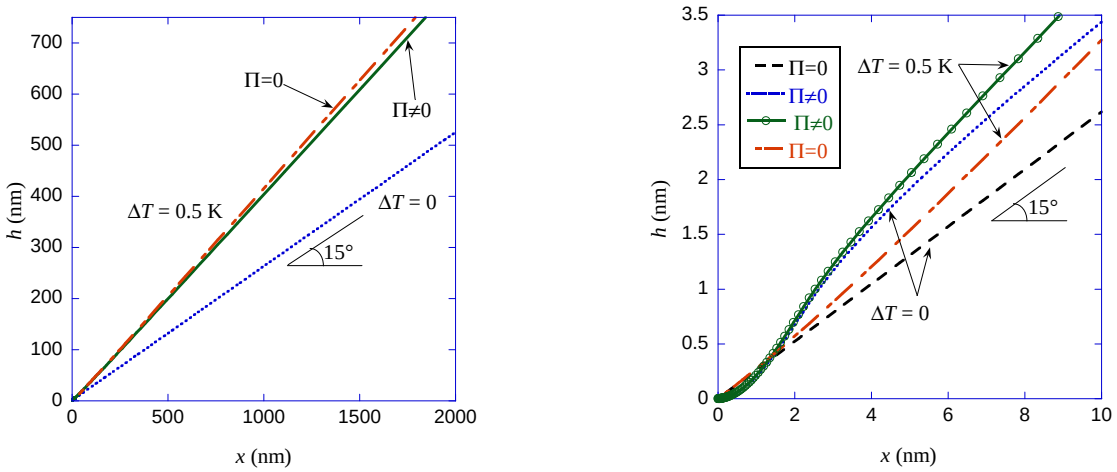

Figure 3: Liquid-vapor interface computed for $\theta_Y = 15°$ with and without disjoining pressure implementation. (a) Large scale. The curves corresponding to $\Pi = 0$ and $\Pi \neq 0$ are indistinguishable at this scale for $\Delta T = 0$. (b) Close contact line vicinity of the curves shown in Fig. (a). The data points for $\Delta T = 0.5$ K, $\Pi \neq 0$ are indicated with circles to illustrate the increasingly dense meshing near the contact line. Note that θ_Y does not correspond to any slope when $\Pi \neq 0$ and $\Delta T \neq 0$.

3b. The variables are assumed to be constant over each element. A BEM mesh at the solid-liquid interface is such that element spacing is consistent with the liquid domain mesh. Total number of elements for the solid domain is 1000. The nonlinearity is treated with the iteration method. The nonlinear terms are replaced by their respective values from the previous iteration.

The material parameters for water at 10 MPa and the stainless steel are used for the calculations. Unless mentioned specifically, $v_{CL} = 0$, $\theta_Y = 15°$, $\theta_{micro} = 1°$, $d_D = 1$ nm, $A = 3.7 \cdot 10^{-20}$ J. According to the review [17], the slip length value varies from 1 nm to 1 μm depending on wettability and the state of the solid surface. For the partial wetting case, l_s is related to the surface roughness. It is assumed that the surface is very smooth and the value $l_s = 10$ nm is adopted. In our computations, we adopt the heater thickness value $D = 90$ nm. It is larger than l_s and another characteristic length scale $k_L R^i \approx 3$ nm associated with R^i (cf. 16). We take such a small value of D to avoid too large x_{max} that must be larger than $L \sim D$.

Examples of computed shape of the liquid-vapor interface with and without accounting for the disjoining pressure are shown in Fig. 3a. The main output of the problem is the slope at $x \to \infty$ that corresponds to the observed (apparent) contact angle θ_{app}. Note that according to its geometrical definition, the curvature is a derivative of the slope over the length measured along the curve, which means (in the small slope approximation adopted here) that

$$\theta_{app} = \theta_{micro} + \int_0^\infty K(x)\mathrm{d}x. \tag{29}$$

Evidently, θ_{app} can be defined only if the integral converges, which is possible if $K(x \to \infty) = 0$. The latter equality is provided by the boundary condition (7) as discussed above. In the calculations with $\Pi = 0$, $\theta_{micro} = \theta_Y$ is chosen to obtain the same macroscopic shape as for $\Pi \neq 0$. The contact line vicinity is zoomed in Fig. 3b. The solution for $\Delta T \neq 0$ is compared with the isothermal shape. Similarly to the complete wetting case, the heating results in an increase of θ_{app}.

The computed pressure difference and the heat flux are shown in Fig. 4 as functions of x. A positive Δp value means that the flow is directed towards the CL. The disjoining pressure account results in an increase of Δp comparing to the solution with $\Pi = 0$. The peak of heat flux is slightly larger for $\Pi \neq 0$ and in both cases the heat flux vanishes when $h \to 0$. The difference in the small scale behaviour for the cases with or without Π introduction is related to the small-scale difference of the wedge shape Fig. 3b. Since the liquid layer thickness is smaller for $\Pi \neq 0$, the heat flux is larger.

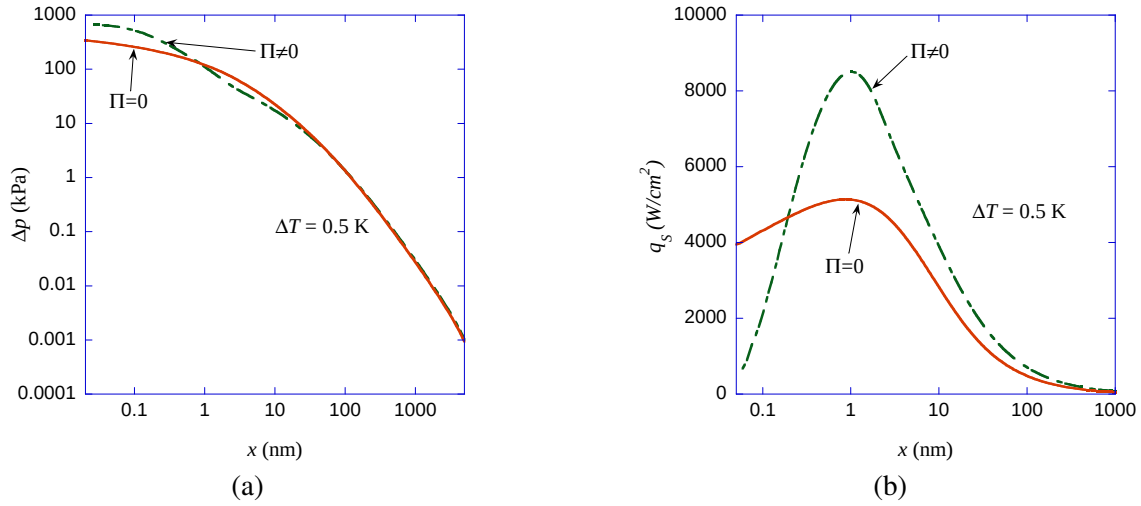

Figure 4: Pressure difference and heat flux distribution for $\Delta T = 0.5$ K and $\theta_Y = 15°$ with and without disjoining pressure account. (a) Pressure difference. (b) Heat flux.

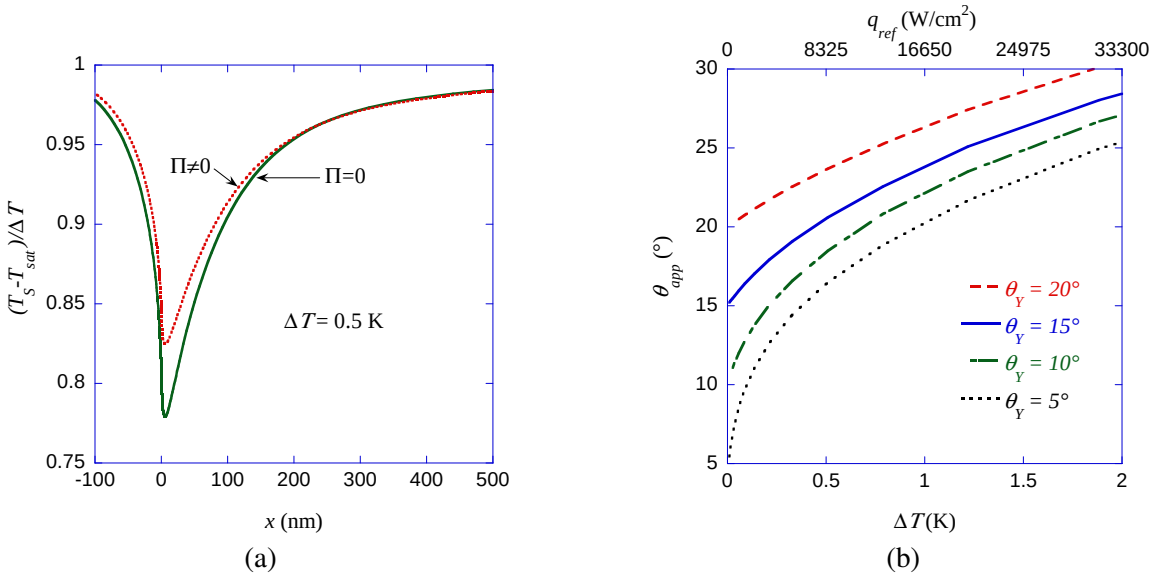

Figure 5: (a) Spatial variation of the temperature T_S of the solid surface. (b) Apparent contact angle θ_{app} as a function of ΔT for $\Pi \neq 0$.

The solid surface temperature is shown in Fig. 5a. The temperature minimum is at $x \approx 2.5$ nm and coincides with the position of the heat flux maximum. The importance of using the non-isothermal approach for the solid heater is evident: $T_S < T_{sat} + \Delta T$ and the heat flux (and θ_{app}) is smaller than the value that would be obtained if the heater surface was imposed to be isothermal at $T_{sat} + \Delta T$. In the agreement with the above analytical analysis, Fig. 5a shows $L \sim D$.

The apparent contact angle θ_{app} is plotted versus ΔT for different θ_Y in Fig. 5b. The trend is similar to the complete wetting case [1–3]: θ_{app} grows with ΔT. It is evident that Young's contact angle θ_Y plays an important role. For small values of θ_Y, a rapid increase of θ_{app} occurs for low ΔT. For $\Delta T > 0.5$ K, the curves for all θ_Y grow with about the same rate. $\theta_{app} - \theta_Y$ can attain 25° for the superheat of 2 K, which is a quite small value. For comparison, a typical value for boiling at moderate heat fluxes is 20 K. One can introduce $q_{ref} = k_S \Delta T / D$ as a characteristic value for the heat flux. The values of q_{ref} corresponding to ΔT are put at the upper axes.

Sensitivity of the results to the parameters of disjoining pressure is analyzed in Fig. 6. It can be seen that the Hamaker constant variation does not affect notably the value of θ_{app}. The maximum of disjoining pressure

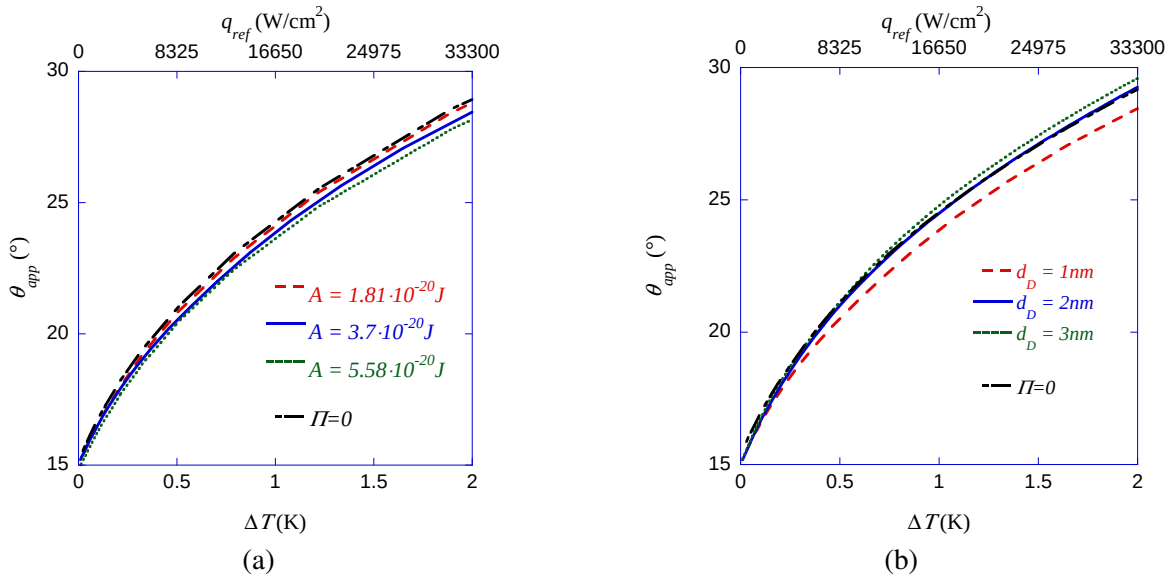

Figure 6: Apparent contact angle θ_{app} versus ΔT for $\theta_Y = 15°$ and different parameters of disjoining pressure. The curve for $\Pi = 0$ is shown for comparison and coincides with curve prescribed to d_D . (a) Hamaker constant variation. (b) Dependence of the position d_D of the maximum of disjoining pressure.

becomes to be lower with A decrease, the influence of Π reduces and the curves approach that for $\Pi = 0$. We verified that the variation of θ_{micro} does not influence θ_{app} notably either.

The influence of the CL motion on θ_{app} is illustrated in Fig. 7a. The capillary number $Ca = v_{CL}\mu/\sigma$ is put at the upper axes for the reference. The difference between the cases with and without disjoining pressure is not significant, and generally speaking the curves are just slightly shifted. Similarly to the case $\Delta T = 0$ discussed in [18], the Landau-Levich (entrainment) transition occurs at a finite $v_{CL} > 0$ and a finite θ_{app} . This means that there is no wedge-like stationary solution for larger velocities (and smaller θ_{app}). The continuous liquid film forms instead.

It is important to know the minimum value of x_{max} required for each particular case. This value is denoted by d_{min}. It should correspond to x where the CL effect on the interface slope becomes negligible, see Fig. 5a. In other words, it is the distance counted from the contact line, at which θ_{app} establishes. It is a priori evident that d_{min} should be at least several times larger than L. From calculations, d_{min} can be determined as a distance at which the interface slope approaches the slope at $x \to \infty$ (equal to θ_{app}) within some accuracy that is choosen to be 10^{-3}. In order to determine d_{min} itself with a sufficient accuracy, $x_{max} \geq 2d_{min}$ is required. Fig. 7b shows d_{min} as a function of v_{CL} for two values of ΔT and θ_Y. For $\Pi = 0$, $d_{min}(\Delta T \to 0) = 0$ because the slope is constant at small scales. For $\Pi \neq 0$, $d_{min}(\Delta T \to 0)$ tends to a constant value that depends on the disjoining pressure: the latter causes the slope variation even at $\Delta T = 0$, see Fig. 3b. Generally, the minimum of the function $d_{min}(v_{CL})$ grows slightly with ΔT for the same θ_Y. The impact of the imposed contact line velocity on the value of d_{min} is very strong: d_{min} grows rapidly with $|v_{CL}|$. This rapid growth is due to weak (logarithmic) convergence [3] of the slope (as a function of x) to θ_{app}.

7. CONCLUSIONS

A 2D model describing hydrodynamics and heat flow in the vicinity of the contact line with the account of the surface forces is developed using the lubrication approximation. It allows to solve the conjugate stationary problems of hydrodynamics and heat transfer in the “micro-region”, a vicinity of the contact line where the main part of the heat and mass transfer takes place and the effect of surface forces might be important and thus need to be studied. This approach can be used to describe many practical situations like bubble dynamics in boiling, menisci motion in the heat pipes, etc.

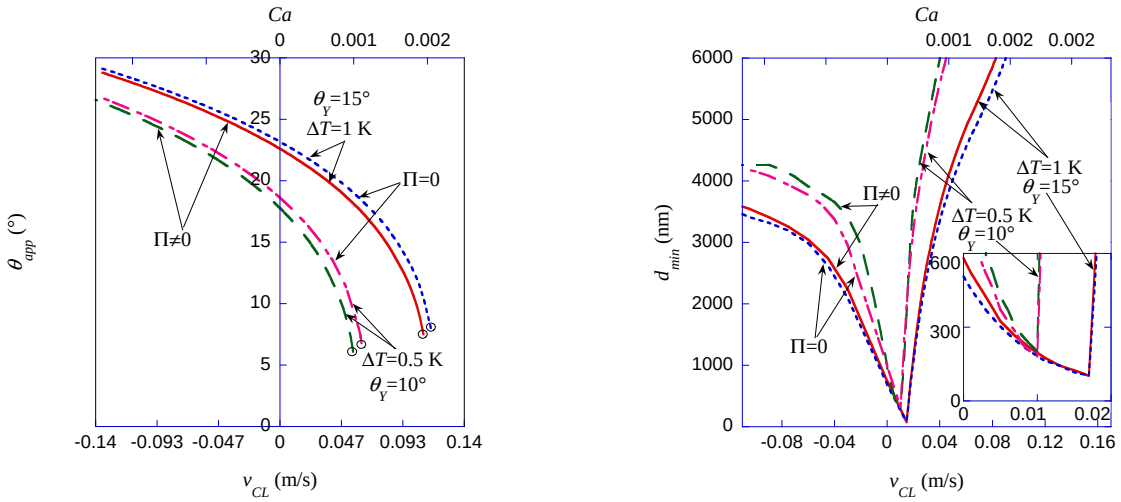

Figure 7: Dependencies on the contact line velocity. The corresponding capillary number is shown in upper axes for $v_{CL} > 0$ (a) Apparent contact angle θ_{app} for $\Delta T = 0.5$, 1 K and $\Pi = 0$, $\Pi \neq 0$. The entrainment transition points are shown with the circles. (b) d_{min} for $\Delta T = 0.5$, 1 K and $\Pi = 0$, $\Pi \neq 0$.

The effects of the heat transfer in solid and liquid phases as well as of the imposed contact line velocity on the value of the apparent contact angle is analyzed. The apparent contact angle rapidly increases with superheating for low values of Young's contact angle. For stronger superheatings the apparent contact angle growth rate is almost independent of the Young contact angle. The effect of the imposed contact line velocity on the apparent contact angle is significant. The general trend agrees with the isothermal case.

A study of various parameters of disjoining pressure shows their relatively weak impact on the apparent contact angle. Therefore, the effect of the surface forces can be considered as negligible in most cases. However, the influence of the heating is strong: even a small substrate superheating of the order of 1 K can lead to a strong increase ($\sim 20°$) of the apparent contact angle.

We analyze the distance at which the apparent contact angle is established. This distance turns out to be of the order 100 nm when the contact line is immobile but grows strongly with the contact line velocity and can attain several μm. This means that the contact angle at nanometric scale should be size dependent.

ACKNOWLEDGEMENTS

The financial support of ANR (project ALICE, ANR-08-BLAN-0212-03) is acknowledged. We are grateful to A. Rednikov, P. Colinet, D. Jamet and B. Mathieu for fruitful discussions.

REFERENCES

[1] P. C. Wayner, Y. K. Kao, and L. V. LaCroix. The interline heat-transfer coefficient of an evaporating wetting film. *Int. J. Heat Mass Transfer*, 19:487 – 492, 1976.

[2] S. J. S. Morris. A phenomenological model for the contact region of an evaporating meniscus on a superheated slab. *J. Fluid Mech.*, 411:59 – 89, 2000.

[3] A. Ye. Rednikov, S. Rossomme, and P. Colinet. Steady microstructure of a contact line for a liquid on a heated surface overlaid with its pure vapor: parametric study for a classical model. *Multiphase Sci. Techn.*, 21(3):213 – 248, 2009.

[4] F. Brochard-Wyart, J.-M. Di Meglio, D. Quere, and P.-G. de Gennes. Spreading of nonvolatile liquids in a continuum picture. *Langmuir*, 7(2):335 – 338, 1991.

[5] N. V. Churaev. Surface forces in wetting films. *Adv. Colloid Interface Sci.*, 103(3):197 – 218, 2003.

[6] P. Stephan and J. Hammer. A new model for nucleate boiling heat transfer. *Heat Mass Transfer*, 30(2):119

– 125, 1985.

[7] J. N. Israelachvili. *Intermolecular and Surface Forces*. Academic Press, London, 2nd edition, 1992.

[8] P.-G. de Gennes, F. Brochard-Wyart, and D. Quéré. *Capillarity and Wetting Phenomena: Drops, Bubbles, Pearls, Waves*. Springer, New York, 2004.

[9] E. K. Yeh, J. Newman, and C. J. Radke. Equilibrium configurations of liquid droplets on solid surfaces under the influence of thin-film forces: Part II. Shape calculations. *Colloids Surf., A*, 156(1-3):525 – 546, 1999.

[10] J. H. Snoeijer and B. Andreotti. A microscopic view on contact angle selection. *Phys. Fluids*, 20(5):057101, 2008.

[11] G. Son, V. K. Dhir, and N. Ramanujapu. Dynamics and heat transfer associated with a single bubble during nucleate boiling on a horizontal surface. *J. Heat Transfer*, 121(3):623 – 631, 1999.

[12] V. S. Ajaev, G. M. Homsy, and S. J. S. Morris. Dynamic response of geometrically constrained vapor bubbles. *J. Colloid Interf. Sci.*, 254(2):346 – 354, 2002.

[13] W. T. Ang. *A Beginner's Course in Boundary Element Methods*. Universal Publishers, Boca Raton, 2007.

[14] A. Oron, S. H. Davis, and S. G. Bankoff. Long-scale evolution of thin liquid films. *Rev. Mod. Phys.*, 69(3):931–980, 1997.

[15] V. S. Nikolayev. Dynamics of the triple contact line on a nonisothermal heater at partial wetting. *Phys. Fluids*, 22(8):082105, 2010.

[16] S. V. Patankar. *Numerical heat transfer and fluid flow*. Hemisphere, Washington, 1980.

[17] E. Lauga, M. P. Brenner, and H. A. Stone. Microfluidics: The no-slip boundary condition. In C. Tropea, A. Yarin, and J. Foss, editors, *Springer Handbook of Experimental Fluid Dynamics*, chapter 19, pages 1217 – 1240. Springer, New York, 2007.

[18] G. Delon, M. Fermigier, J.H. Snoeijer, and B. Andreotti. Relaxation of a dewetting contact line. Part 2: Experiments. *J. Fluid Mech.*, 604:55 – 75, 2008.